Journal of Zhejiang University-SCIENCE A (Applied Physics & Engineering)
ISSN 1673-565X (Print); ISSN 1862-1775 (Online)
www.zju.edu.cn/jzus; www.springerlink.com
E-mail: jzus@zju.edu.cn

Digital simulation of 3D turbulence wind field of Sutong Bridge based on measured wind spectra*

Hao WANG†[1,2], Zhou-hong ZONG[1], Ai-qun LI[1,2], Teng TONG[1], Jie NIU[1], Wen-ping DENG[1,2]

([1]*Key Laboratory of Concrete and Prestressed Concrete Structures of Ministry of Education, Southeast University, Nanjing 210096, China*)

([2]*Key Laboratory of Environmental Impact and Structural Safety in Engineering, China University of Mining & Technology, Xuzhou 221116, China*)

†E-mail: whzjn@sina.com

Received July 7, 2011; Revision accepted Sept. 23, 2011; Crosschecked Dec. 29, 2011

Abstract: Time domain analysis is an essential implement to study the buffeting behavior of long-span bridges for it can consider the non-linear effect which is significant in long-span bridges. The prerequisite of time domain analysis is the accurate description of 3D turbulence winds. In this paper, some hypotheses for simplifying the 3D turbulence simulation of long-span cable-stayed bridges are conducted, considering the structural characteristics. The turbulence wind which is a 3D multivariate stochastic vector process is converted into four independent 1D univariate stochastic processes. Based on recorded wind data from structural health monitoring system (SHMS) of the Sutong Bridge, China, the measured spectra expressions are then presented using the nonlinear least-squares fitting method. Turbulence winds at the Sutong Bridge site are simulated based on the spectral representation method and the Fast Fourier transform (FFT) technique, and the relevant results derived from target spectra including measured spectra and recommended spectra are compared. The reliability and accuracy of the presented turbulence simulation method are validated through comparisons between simulated and target spectra (measured and recommended spectra). The obtained turbulence simulations can not only serve further analysis of the buffeting behavior of the Sutong Bridge, but references for structural anti-wind design in adjacent regions.

Key words: Turbulence simulation, Spectral representation method, Fast Fourier transform (FFT), Cable-stayed bridges, Structural health monitoring system (SHMS), Power spectral density

doi:10.1631/jzus.A1100177 **Document code:** A **CLC number:** U448.27

1 Introduction

Long-span bridges such as cable-stayed and suspension bridges are vulnerable to wind-induced vibrations. The aerostatic and aerodynamic behaviors of these bridges under strong winds have been the concern of engineers for a long time (Davenport, 1962; Bocciolone *et al.*, 1992; Bartoli and Mannini, 2008; Øiseth *et al.*, 2010; Wang *et al.*, 2010a). Among them, bridge buffeting, induced by turbulence winds, is becoming of greater concern for that this would be significant with the rising span and the broadening deck (Scanlan, 1978; Katsuchi *et al.*, 1999; Xu *et al.*, 2000; Wang *et al.*, 2011). To combat bridge buffeting, analyses in frequency (Simiu and Scanlan, 1978) and time domain (Kovacs *et al.*, 1992) are two general approaches. Analysis in frequency domain about dynamic responses under stochastic winds can be realized by numerically integrating the product of the bridge's transfer function and the wind load spectra (Yang *et al.*, 1997). However, the prerequisite of the methodology is the linear hypothesis, which indicates its unsuitability to most of

* Project supported by the National Natural Science Foundation of China (Nos. 50725828, 50908046, and 50978056), the Teaching & Scientific Research Fund for Excellent Young Teachers of Southeast University, the Open Fund of Jiangsu Key Laboratory of Environmental Impact and Structural Safety in Engineering, the Basic Scientific & Research Fund of Southeast University (No. Seucx-201106), and the Priority Academic Program Development Foundation of Jiangsu Higher Education Institutions, China

long-span bridges, for that, flexibilities and nonlinear behaviors resulted from either geometrical or aerodynamic effects are apparent in these bridges (Niemann and Hoffer, 1995; Yang *et al.*, 1997; Su *et al.*, 2007). Conversely, time domain analysis, employing step-by-step numerical integration, is the only choice for resolving nonlinear aerodynamic responses of long-span bridges. To conduct time domain analysis, wind load histories at bridge sites are important for accurate simulation since aerodynamic behaviors are sensitive to the selected winds (Bocciolone *et al.*, 1992; Chen *et al.*, 2000).

As for certain stochastic issues involved in nonlinearity, large variations of uncertain parameters, etc., the Monte Carlo method seems to be the only universal method that can provide accurate solutions (George, 1996). The core task of the methodology is to generate sample functions of stochastic processes. The auto-regressive and moving average (ARMA) method (Li and Kareem, 1993; Di Paola, 1998) and spectral representation method (Shinozuka, 1972) are mainly adopted to produce such sample functions. The ARMA method offers a computationally efficient scheme which does not require large computer storage whereas crude calculated results are obtained. Conversely, the spectral representation method, although with computationally expensive efforts, is mostly adopted since it can produce unconditionally stable results (Yang *et al.*, 1997). Shinozuka (1972) and Shinozuka and Jan (1972) first applied the spectral representation method to simulate multidimensional, multivariate and non-stationary cases. Yang (1972; 1973) combined it with the fast Fourier transform (FFT) technique and the computational efficiency of the spectral representation algorithm is drastically improved. Since then, the spectral representation method combined with the FFT technique achieved rapid development and many researchers made considerable contributions to refine this methodology in various arenas (Li and Kareem, 1993; Yamazaki and Shinozuka, 1998).

In this paper, turbulence simulations are conducted for the Sutong Bridge in China which is the longest cable-stayed bridge globally so far, employing the spectral representation method and the FFT technique. Sample functions of turbulence velocities and turbulence power spectra are generated with the assistance of the measured wind data from the structural health monitoring system (SHMS). Some hypotheses and improvements are adopted to simplify and refine the relevant simulations for the main girder and towers, respectively. Specifically, it is assumed that the girder is on the same elevation and the wind field is homogeneous along the spanwise direction of the bridge, which means winds are evenly distributed along the bridge span. The improvement is taken which considers non-uniform wind distribution along the vertical direction to refine turbulence simulations for towers. The accuracy of obtained results is validated by comparing them with those derived from the current specification (Xiang *et al.*, 2004). Turbulence simulations in this paper can provide not only reliable turbulence data for further analysis of buffeting behavior of the Sutong Bridge, but references for anti-wind design of structures in adjacent regions.

2 Related works

2.1 Description of Sutong Bridge

Sutong Bridge (Fig. 1) connects Suzhou and Nantong cities of Jiangsu Province with the main span of 1088 m. The bridge construction was initiated in June, 2003 and opened to the public on May 25, 2008.

The stream-line flat steel-box girder, with the overall width including the two wind mouths of 41.0 m and the height at the centerline of 4.0 m, is employed in the Sutong Bridge. The two main towers are inverted Y-shaped, including upper columns, middle columns, lower columns and lower beams. The overall height of towers is 300.40 m, and 230.41 m of the total height is above the main girder, and are the world's tallest bridge towers. Parallel wire cables with intervals being 16 and 2 m on the deck and towers respectively are adopted, and the total number

Fig. 1 The Sutong Bridge, China

of cables is 272. Among them, the longest cable is 577 m with the largest size of PES7-313 (polyethylene extrusion cable with 313 steel wires of 7 mm in diameter), which is a record-breaking stayed-cable. Horizontal anti-wind bearings and vertical viscous dampers are installed at the junction of the main girder and towers. For the two enormous foundations, 131 bored piles with the inner diameter of steel tubes being 2.8 m are constructed to support each tower. The configuration of the bridge is schematically shown in Fig. 2.

2.2 Climate and SHMS

Sutong Bridge is located at the lower reach of the Yangtze River and towards the sea (Fig. 3). The meteorological survey reveals that this region is dominated by a humid subtropical monsoon climate. Prior to the construction, anti-wind design is mainly according to in-field measurement by the local meteorological department (Liu *et al.*, 2006), as well as wind tunnel aeroelastic model (1:85) of full bridge (Chen, 2004). Nevertheless, both of them are insufficient for buffeting analysis of the real bridge.

To monitor and assess bridge conditions during the constructing and operating periods, especially under extreme events such as typhoons, heavy snow falls, heavy traffic, etc., the SHMS is installed (Wang *et al.*, 2010a). The SHMS with anemometers is a powerful implement for studying wind characteristics. Fig. 4 shows the layout of sensors in the SHMS in the Sutong Bridge. The SHMS has four sub-systems including the sensory, data acquisition and transferring, data managing and controlling, and structural health estimation systems. There are in total 15 types of sensors ensuring measurements of different loads and effects on the bridge. The number in the bracket indicates the sensor quantity. For wind measurements, four 3D ultrasonic anemometers are installed. Two of them are installed in upstream and downstream sides respectively at the midpoint (76 m in elevation). The others are at the top of the south and north towers (306 m in elevation).

3 Simulation of stationary stochastic vector process

Natural winds are divided into two components which are mean and turbulence winds (Simiu and Scanlan, 1978). Turbulence wind, average velocity equals zero, is not only a function of time, but varies with the spatial location (x, y, z), namely a 1D and 4-variate (1D-4V) stationary stochastic vector process. The spectral representation method combined with the FFT technique (George, 1996) is generally adopted to deal with such processes.

Fig. 3 Location of the Sutong Bridge

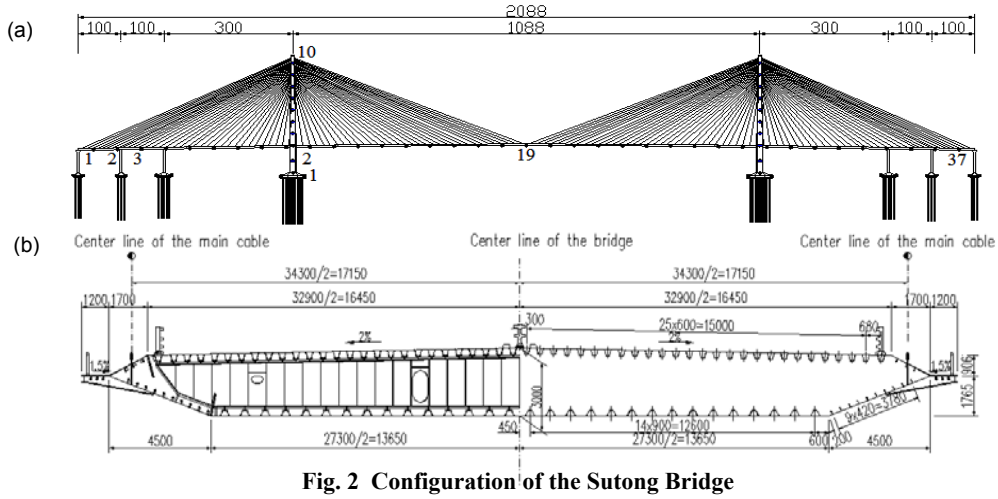

Fig. 2 Configuration of the Sutong Bridge
(a) Elevation (unit: m); (b) Cross-section of the steel box girder (unit: mm)

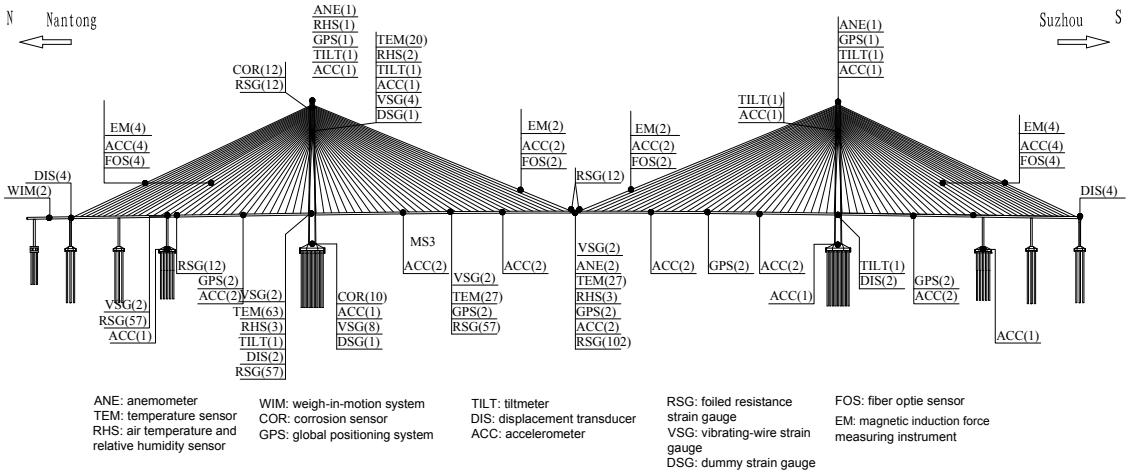

Fig. 4 Wind direction frequency of the largest daily wind speed

3.1 Spectral representation method

Consider a 1D, n-variate (1D-nV) stationary stochastic vector process with components of $f_1^0(t)$, $f_2^0(t)$, …, $f_n^0(t)$, having average values equal to zero, and the superscript "0" denotes the target functions.

$$E\left[f_j^0(t)\right]=0,\quad j=1,2,...n, \tag{1}$$

the cross-correlation matrix is

$$\boldsymbol{R}^0(\tau)=\begin{bmatrix} R_{11}^0(\tau) & R_{12}^0(\tau) & \cdots & R_{1n}^0(\tau) \\ R_{12}^0(\tau) & R_{22}^0(\tau) & \cdots & R_{2n}^0(\tau) \\ \vdots & \vdots & & \vdots \\ R_{n1}^0(\tau) & R_{n2}^0(\tau) & \cdots & R_{nn}^0(\tau) \end{bmatrix}, \tag{2}$$

and the cross-spectral density matrix is

$$\boldsymbol{S}^0(\omega)=\begin{bmatrix} S_{11}^0(\omega) & S_{12}^0(\omega) & \cdots & S_{1n}^0(\omega) \\ S_{12}^0(\omega) & S_{22}^0(\omega) & \cdots & S_{2n}^0(\omega) \\ \vdots & \vdots & & \vdots \\ S_{n1}^0(\omega) & S_{n2}^0(\omega) & \cdots & S_{nn}^0(\omega) \end{bmatrix}. \tag{3}$$

To simulate the 1D-nV stationary stochastic process $f_j^0(t)$, j=1,2,…, n, the cross-spectral density matrix $\boldsymbol{S}^0(\omega)$ must be divided into the following products:

$$\boldsymbol{S}^0(\omega)=\boldsymbol{H}(\omega)\boldsymbol{H}^{\mathrm{T}*}(\omega). \tag{4}$$

The division can be performed through Cholesky's method, in which case $\boldsymbol{H}(\omega)$ is a lower triangular matrix. $\boldsymbol{H}(\omega)$ is

$$\boldsymbol{H}(\omega)=\begin{bmatrix} H_{11}(\omega) & 0 & \cdots & 0 \\ H_{12}(\omega) & H_{22}(\omega) & \cdots & 0 \\ \vdots & \vdots & & \vdots \\ H_{n1}(\omega) & H_{n2}(\omega) & \cdots & H_{nn}(\omega) \end{bmatrix}, \tag{5}$$

whose diagonal elements are real and non-negative functions of ω, and off-diagonal elements are generally complex functions of ω. The following relations are validated for the elements of matrix $\boldsymbol{H}(\omega)$:

$$H_{jj}(\omega)=H_{jj}(-\omega),\quad j=1,2,...,n, \tag{6}$$

$$H_{jk}(\omega)=H_{jk}^*(-\omega),\quad j=2,3,\ k=1,2,\ j>k. \tag{7}$$

The off-diagonal elements $H_{jk}(\omega)$ can be written in polar form as

$$H_{jk}(\omega)=\left|H_{jk}(\omega)\right|\mathrm{e}^{\mathrm{i}\theta_{jm}(\omega)},\quad j=2,3,\ k=1,2,\ j>k, \tag{8}$$

where

$$\theta_{jm}(\omega)=\tan^{-1}\left\{\frac{\mathrm{Im}\left[H_{jm}(\omega)\right]}{\mathrm{Re}\left[H_{jm}(\omega)\right]}\right\}. \tag{9}$$

Once the matrix $\boldsymbol{S}^0(\omega)$ is divided, the stochastic process can be simulated by the following series as $N\to\infty$:

$$f_j(t)=2\sum_{m=1}^{j}\sum_{l=1}^{N}\left|H_{jk}(\omega)\right|\sqrt{\Delta\omega}\cos\left(\omega_{ml}-\theta_{jm}\left(\omega_{ml}\right)+\phi_{ml}\right),\quad j=1,2,...,n, \tag{10}$$

where

$$\omega_{ml}=(l-1)\Delta\omega+\frac{m}{n}\Delta\omega,\ j=1,2,...,N, \tag{11}$$

$$\Delta\omega=\omega_{\mathrm{u}}/N, \tag{12}$$

where l denotes one of the number of FFT points, N is the frequency segment, ω_{u} denotes the upper cutoff frequency beyond which the elements of the cross-spectral density matrix may be assumed to be zero for either mathematical or physical reasons, and φ_{ml} are sequences of independent random phase angles distributed uniformly over the interval from 0 to 2π.

When generating sample functions of the simulated stochastic process according to Eq. (10), the time step Δt separating the generated values in time domain must satisfy the demand to avoid aliasing:

$$\Delta t\le\frac{2\pi}{2\omega_{\mathrm{u}}}. \tag{13}$$

The period T_0 of simulated stochastic process is

$$T_0=\frac{2\pi n}{\Delta\omega}=\frac{2\pi nN}{\omega_{\mathrm{u}}}. \tag{14}$$

From the above description, it can be concluded that sampling functions of a stochastic process can be obtained, with the known $\boldsymbol{S}^0(\omega)$ and adequate selection of N, ω_{u} and Δt.

3.2 FFT technique

The cost of digitally generation of sample functions of the simulated stochastic vector process can be drastically reduced by the FFT technique. To achieve this, Eq. (10) should be written as

$$f_j(p\Delta t)=\mathrm{Re}\left\{\sum_{m=1}^{j}h_{jm}(q\Delta t)\exp\left[\mathrm{i}\left(\frac{m\Delta\omega}{3}\right)(p\Delta t)\right]\right\},$$

$$p=0,1,\cdots,2N\times n-1,\ j=1,2,\cdots,n, \tag{15}$$

where q is the remainder of $p/(2N)$, q=0,1,⋯,n−1, and $h_{jm}(q\Delta t)$ is given by

$$h_{jm}(q\Delta t)=\sum_{l=1}^{2N-1}B_{jm}(l\Delta\omega)\exp\left(\mathrm{i}\frac{\pi lq}{N}\right), \tag{16}$$

$$B_{jm}(l\Delta\omega)=\begin{cases}\sqrt{2(\Delta\omega)}H_{jm}\left(l\Delta\omega+\dfrac{m\Delta\omega}{n}\right)\exp(\mathrm{i}\varphi_{ml}),\ 0\le l<N,\\ 0,\ N\le l<2N.\end{cases} \tag{17}$$

From the above equations, it shows that $h_{jm}(q\Delta t)$ is the Fourier transform of $B_{jm}(l\Delta\omega)$. Thus, the FFT technique can be used in simulations of turbulence winds with the spectral representation method.

4 Hypotheses for wind field simulation

4.1 Simplified wind fields for long-span bridges

Natural winds can be divided into two components: mean and turbulence winds:

$$\begin{cases}U=\bar{U}(Z)+u(x,Z,t),\\ v=v(x,Z,t),\\ w=w(x,Z,t),\\ 0<x\le L,\ 0<Z\le H,\end{cases} \tag{18}$$

where u, v and w are turbulence winds in across-bridge, along-bridge and vertical directions, respectively; $\bar{U}(Z)$ is the mean wind velocity in across-bridge direction; L is the span of bridges and H is the tower height.

The continuous wind fields should be divided into finite components to facilitate the calculation. As the correlations between the three turbulence parts in x, y and z directions are negligible, they are not considered in practical terms. Only the correlation in spatial distributions of turbulence winds is taken into account. Wind fields can therefore be divided into three independent 1D components in x, y and z directions, which is a process of converting a 3D multi-variate (3D-nV) stochastic vector process into

three independent 1D multi-variate (1D-*n*V) stochastic processes.

Turbulence simulations for large-scale structures are complicated because of the numerous simulated points. Consider the structural characteristics of each type of long-span bridges (cable-stayed and suspension bridges), some hypotheses can be construed to improve the calculation. Specifically, in suspension bridges, the main girder is the primary component subjected to wind loads and the coupled vibrations of the main girder and towers are negligible, indicating that mere simulations of wind fields of the main girder can generate accurate results. However, for cable-stayed bridges, the coupled vibrations between the main girder and towers are intense. In addition, towers in cable-stayed bridges are larger than counterparts in suspension bridges, meaning that the towers are more prone to wind loads. Hence, neglecting the wind fields of towers in cable-stayed bridges would be inappropriate.

4.2 Simulation of wind fields

As mentioned above, for long-span cable-stayed bridges, wind simulations for the main girder and towers should be undertaken. Specifically, for the main girder, turbulence simulation in along-bridge direction (*v*) is not considered as the main girder is the linear component in the direction. For towers, turbulence simulations in along-bridge direction (*v*) are not considered as towers are intensively constrained by the main girder and cables, which means along-bridge vibrations are greatly affected by the main girder and cables and influences from turbulence winds are negligible in this direction. Turbulence simulation in vertical direction (*w*) for towers is also not considered (Han *et al*., 2003; Wang *et al*., 2010b). Therefore, four independent 1D univariate (1D-1V) stochastic processes can be assumed for the Sutong Bridge according to hypotheses above, listed in Table 1.

The layout of simulated points in the Sutong Bridge is schematically shown in Fig. 5. There are 37 simulated points (from G1 to G37) uniformly distributed along the main girder, with the interval being 56 m. Similarly, there are 10 simulated points (from T1 to T10) in the left tower distributed uniformly along each tower, with intervals being 30 m.

5 Turbulence simulations for Sutong Bridge

To conduct turbulence simulations by the spectral representation method and the FFT technique (George, 1996), the selection of power spectra is indispensable. There already exist certain turbulence power spectra, e.g., the Davenport spectrum, Kaimal spectrum, and Kaman spectrum. Nevertheless, these spectra are not homogenous and some apparent differences appear, leading to the questionable simulated wind fields (Wang *et al.*, 2010b). In the following simulations, the turbulence power spectra rely on the measured wind data from the SHMS. In addition, the adverse effects, such as mechanical filtering of the anemometers and the influence of the sampling rate, are removed prior to comparing with theoretical spectra (Beljaars, 1987; Gurley and Kareem, 1993).

5.1 Wind spectra

The distribution of the mean wind velocity with the attitude at the Sutong Bridge site is consistent with the power law (Hu *et al.*, 2010):

Table 1 1D-1V stochastic wind fields for the Sutong Bridge

Wind field	Position	Direction	Space Interval (m)	Number of simulated nodes
1	Main girder	*u*	56	37
2	Main girder	*w*	56	37
3	Left tower	*u*	30	10
4	Right tower	*u*	30	10

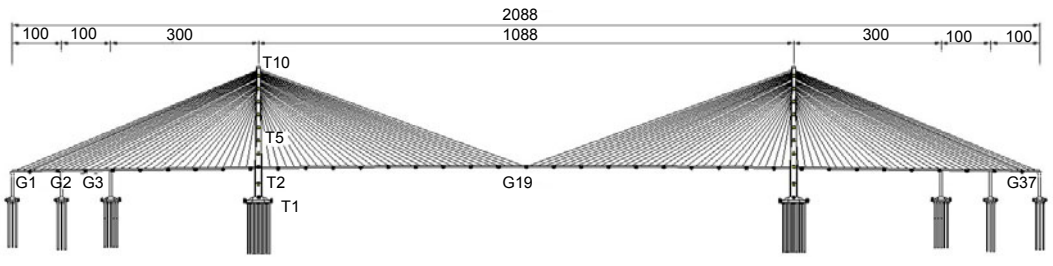

Fig. 5 Simulated points of the Sutong Bridge (unit: m)

$$\frac{U_2}{U_1}=\left(\frac{Z_2}{Z_1}\right)^{\alpha}, \tag{19}$$

where U_1 and U_2 denote wind velocities at the height Z_1 and Z_2 above the ground, respectively, and α is a dimensionless exponent dependent upon roughness of terrain, taken as measured value 0.12 herein (Wang *et al.*, 2010a).

The power spectra are obtained by fitting the wind velocity records to the objective function. The wind records are from field measurements of Typhoon Fung-Wong, Typhoon Kalmaegi (Hu *et al.*, 2010) and strong winter winds (Wang *et al.*, 2010a), using the nonlinear least squares method (Strutz, 2010). In along-wind direction, the objective function takes the form like the Kaimal spectrum (Kaimal *et al.*, 1972):

$$\frac{nS_{\mathrm{u}}(n)}{(u^*)^2}=\frac{af}{(1+bf)^{5\beta/3}}, \tag{20}$$

where a, b and β are parameters to be fitted; f is the Moning coordinates, and u^* is the wind friction speed. f and u^* can be further expressed as below:

$$f=nZ/U, \tag{21}$$

$$u^*=kU(Z)/\ln(Z/Z_0). \tag{22}$$

where n is the frequency of the wind speed, and Z_0 is the roughness length.

For the Sutong Bridge, based on the measured wind data, the parameters are fitted as: $U(Z)$= 15.6986 m/s, k=0.4, Z_0=0.01, Z=75.59 m and u^*=0.703. Therefore, a=90.2, b=58.5 and β=0.95 can be obtained whereas in the Kaimal spectrum the parameters are a=200, b=50, and β=1. Their comparisons are plotted in Fig. 6.

Similarly, based on the data measure for three strong winds, the initial fit equation for the across-wind turbulence wind power spectrum density function can be taken as the Panofsky spectrum (Panofsky and McCormick, 1960):

$$\frac{nS_{\mathrm{w}}}{u^{*2}}=\frac{af}{(1+bf)^{2\beta}}. \tag{23}$$

The parameters are fitted as: $U(Z)$=15.6986 m/s, k=0.4, Z_0=0.01, Z=75.59 m and u^*=0.703. Therefore, a=2.1, b=1.6, and β=0.80 can be obtained whereas in Panofsky spectrum the parameters are a=6, b=4, and β=1. Their comparisons are plotted in Fig. 7.

Figs. 6 and 7 reveal an apparent discrepancy between the fitted/measured power spectra and the recommended power spectra in both along-wind and vertical directions, validating the importance of the measured data from the SHMS.

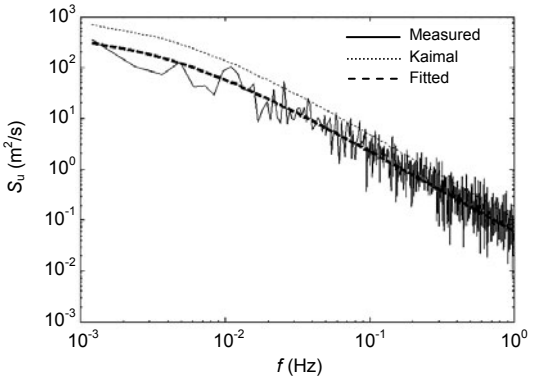

Fig. 6 Turbulence wind power spectra in along-wind direction

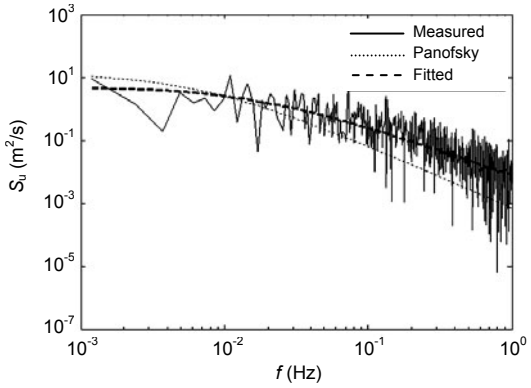

Fig. 7 Turbulence wind power spectra in vertical direction

5.2 Turbulence simulation for main girder

5.2.1 Modified spectral representation method for main girder

Eq. (3) is practically converted into a real matrix. With turbulence simulations for the main girder being taken into consideration, further hypothesis which assumes the turbulence spectra as constant at the identical elevation can be conducted (Cao *et al.*, 2000):

$$S_{11}^0(\omega)=S_{22}^0(\omega)=\ldots=S_{nn}^0(\omega)=S(\omega), \tag{24}$$

$$S_{jm}^{0}(\omega)=\sqrt{S_{jj}^{0}(\omega)S_{mm}^{0}(\omega)}\mathrm{Coh}\left(\Delta_{jm},\omega\right)=S(\omega)\mathrm{Coh}\left(\Delta_{jm},\omega\right), \tag{25}$$

where Δ_{jm} is the distance between points j and m which are at the same height, $\mathrm{Coh}(\Delta_{jm},\omega)$ is the coherence function. Consider that the simulated points in the Sutong Bridge are distributed uniformly in the main girder and the horizontal distance between points j and m is $\Delta_{jm}=\Delta|j-m|$, then the coherence function recommended by Davenport can be written as

$$\mathrm{Coh}\left(\Delta_{jm},\omega\right)=\exp\left(-\frac{\lambda\omega\Delta_{jm}}{2\pi U(Z)}\right)=\exp\left(-\frac{\lambda\omega\Delta|j-m|}{2\pi U(Z)}\right)=\left(\exp\left(-\frac{\lambda\omega\Delta}{2\pi U(Z)}\right)\right)^{|j-m|}=C^{|j-m|}, \tag{26}$$

where λ=7–10 denotes the reducing factor for turbulence winds in across-bridge direction. Substituting Eqs. (24)–(26) into Eq. (3), we can obtain

$$\boldsymbol{S}^{0}(\omega)=\boldsymbol{S}(\omega)=\begin{bmatrix}1 & C & C^{2} & \cdots & C^{n-1}\\ C & 1 & C & \cdots & C^{n-2}\\ C^{2} & C & 1 & \cdots & C^{n-3}\\ \vdots & \vdots & \vdots & & \vdots\\ C^{n-1} & C^{n-2} & C^{n-3} & \cdots & 1\end{bmatrix}. \tag{27}$$

Converting Eq. (27) into an explicit approach:

$$\boldsymbol{H}(\omega)=\sqrt{\boldsymbol{S}(\omega)}\boldsymbol{G}(\omega), \tag{28}$$

where

$$\boldsymbol{G}(\omega)=\begin{bmatrix}1 & & & & & 0\\ C & \sqrt{1-C^{2}} & & & & \\ C^{2} & C\sqrt{1-C^{2}} & \sqrt{1-C^{2}} & & & \\ C^{3} & C^{2}\sqrt{1-C^{2}} & C\sqrt{1-C^{2}} & \sqrt{1-C^{2}} & & \\ \vdots & \vdots & \vdots & \vdots & \sqrt{1-C^{2}} & \\ C^{(n-1)} & C^{(n-2)}\sqrt{1-C^{2}} & C^{(n-3)}\sqrt{1-C^{2}} & C^{(n-4)}\sqrt{1-C^{2}} & \cdots & \sqrt{1-C^{2}}\end{bmatrix}. \tag{29}$$

Converting Eq. (29) into an analytical formula:

$$G_{jm}(\omega)=\begin{cases}0, & 1\le j<m\le n,\\ C^{|j-m|}, & m=1,\ m\le j\le n,\\ C^{|j-m|}\sqrt{(1-C^{2})}, & 2\le m\le j\le n,\end{cases} \tag{30}$$

for that $0<C<1$, the matrix $\boldsymbol{H}(\omega)$ is therefore a real matrix. Hence,

$$\boldsymbol{H}^{\mathrm{T}*}(\omega)=\boldsymbol{H}^{\mathrm{T}}(\omega), \tag{31}$$

$$\theta_{jm}=0. \tag{32}$$

5.2.2 Turbulence simulation

Turbulence simulations for the main girder in along-wind and vertical directions are generated by the modified spectral representation method and the FFT technique. The Davenport coherence function (Simiu and Scanlan, 1978) is adopted with λ being 7. The measured spectra and recommend spectra in current specification (Xiang *et al.*, 2004) are employed to carry out the comparison. Details involved in simulations are listed in Table 2.

Table 2 Details for turbulence simulations of main girder

Parameter	Value	Parameter	Value
Overall length, L (m)	2088	Height of midpoint, Z (m)	75.59
Number of simulated points, n	37	Upper cutoff frequency, ω_u (rad/s)	10π
Frequency segmentations, N	2048	Sample interval, Δt (s)	0.1
Sample period, T_0 (s)	15 155	Simulated time, T_u (s)	1200

Turbulence simulations for 3D wind fields are achieved by Matlab. In the spectral analysis, the size of FFT technology is 1024 with a frequency increment of 0.00175 Hz between two adjacent data points, the piecewise smoothing method and the Hamming window are adopted and the nonlinear least squares fitting technique is used to reduce the random error of spectral estimates. Turbulence velocities in along-wind and vertical directions based on the recommended and fitted spectra are shown in Figs. 8 and 9, respectively. Note that the selection of simulated points is points G1 and G19 located at the left side and midpoint of the Sutong Bridge (Fig. 5).

Comparisons between the simulated spectra of selected points (points G1, G2, G19 and G37, refer to Fig. 5) and the Kaimal spectrum, as well as the simulated spectra of selected points and the fitted spectrum in along-wind direction are shown in Fig. 10 (p.100). In addition, comparisons between the simulated spectra of selected points and the Panofsky spectrum, as well as the simulated spectra of selected points and the fitted spectrum in vertical direction are

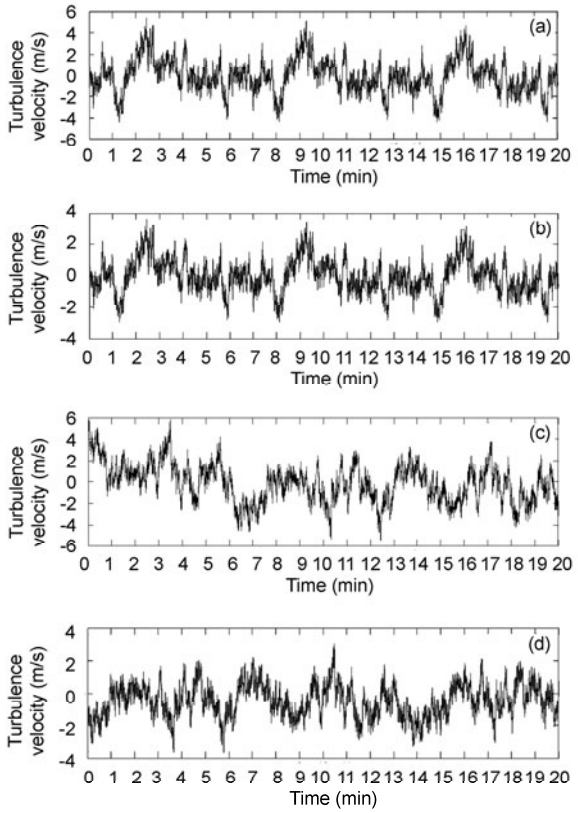

Fig. 8 Simulation of turbulence velocity for main girder in alone-wind direction

Kaimal (a) and fitted (b) spectra for point G1; Kaimal (c) and fitted (d) spectra for point G19

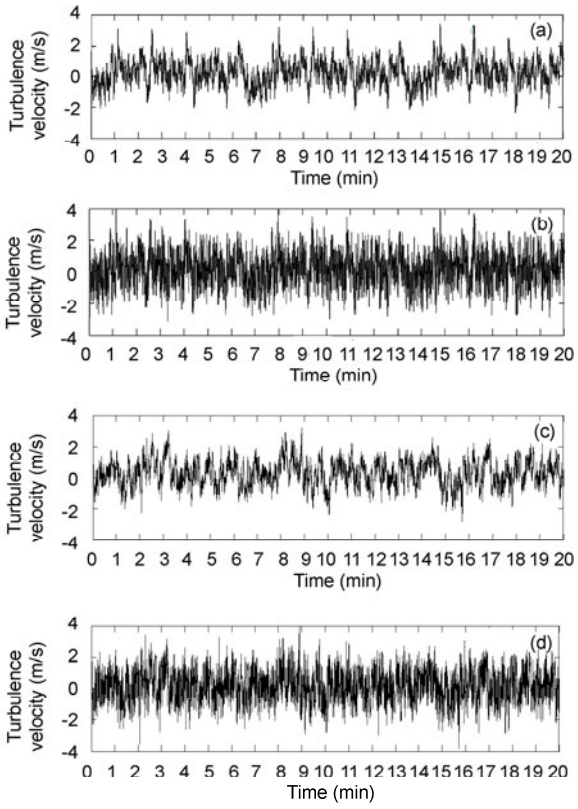

Fig. 9 Simulation of turbulence velocity for main girder in vertical direction

Panofsky (a) and fitted (b) spectra for point G1; Panofsky (c) and fitted (d) spectra for point G19

shown in Fig. 11. The supplement of points G2 and G37 primarily considers the comparison of correlations between points spatially distributed, for that points G2 and G37 are the nearest and farthest ones from point G1. Overall, it can be concluded that the simulated spectra of points G1, G2, G19 and G37 match well with the Kaimal spectrum or fitted spectrum, signifying the reliability of the measured wind data.

Furthermore, comparisons for temporal auto-/cross-correlation functions between generated sample functions and fitting spectrum in along-wind and vertical directions are shown in Figs. 12 and 13. Through comparing values of auto-correlation (point G1) and cross-correlation (points G1 and G19) functions, it is indicated that the correlation of the wind velocities at two points reduces as the distance between two points increases. The effectiveness and reliability of the methodology applied for spatial wind simulation are also validated.

5.3 Turbulence simulation for towers

5.3.1 Modified spectral representation method for towers

In turbulence simulation for towers, the wind velocity is generally assumed to be identical along the tower, which means that different phase angles are not considered. This hypothesis leads the cross spectral density matrix to be a real symmetric positive matrix, simplifying the relative analysis. However, the distribution of the wind velocity is approximately consistent with the exponential relationship (Eq. (19)), and the discrepancy will be more significant with high towers being regarded. Therefore, turbulence simulations for long-span cable-stayed bridges' towers should take this discrepancy into account. The cross spectral density matrix will be a complex and non-positive matrix, proposing difficulties for simulation. In general cases, the turbulence spectral density function is

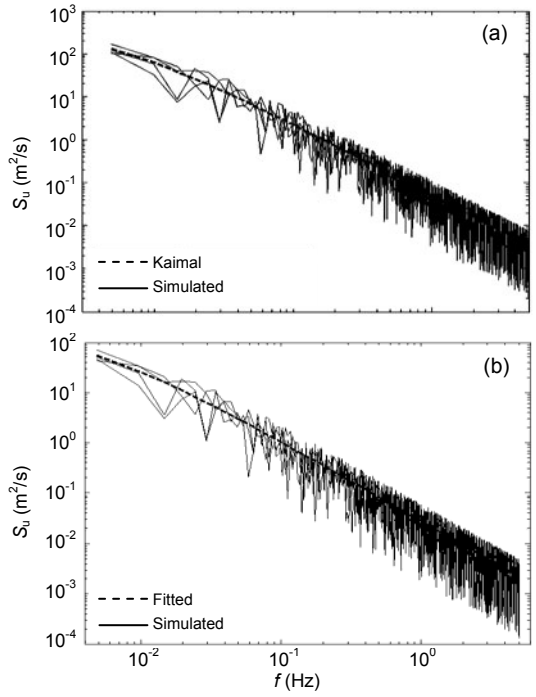

Fig. 10 Comparison of power spectra in along-wind direction
(a) Simulated (points G1, G2, G19 and G37) and Kaimal spectra; (b) Simulated (points G1, G2, G19 and G37) and fitted spectra

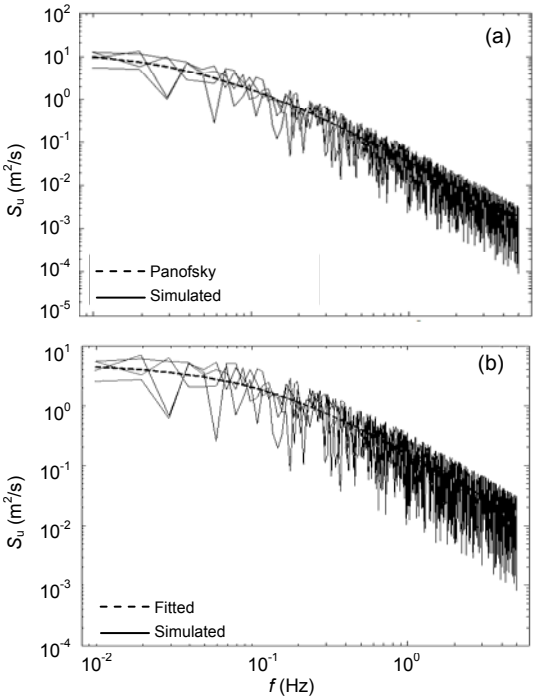

Fig. 11 Comparison of power spectra in vertical direction
(a) Simulated (points G1, G2, G19 and G37) and Panofsky spectra; (b) Simulated (points G1, G2, G19 and G37) and fitted spectra

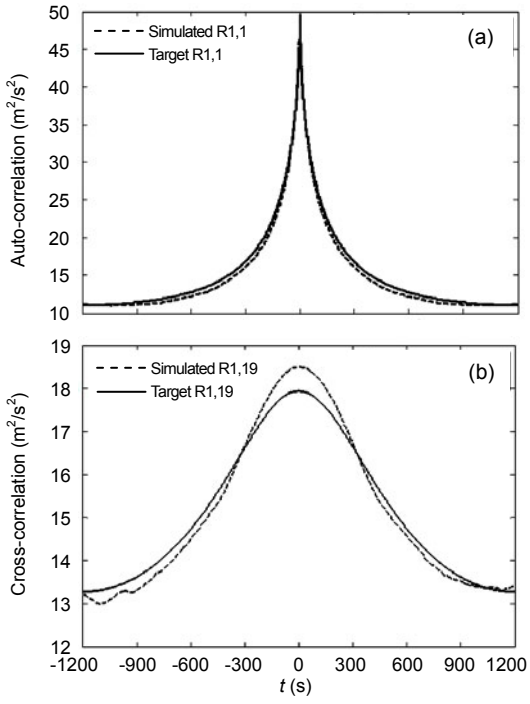

Fig. 12 Comparison of correlation in along-wind direction (target: Kaimal spectrum)
(a) Auto-correlation function (point G1); (b) Cross-correlation function (points G1 and G19)

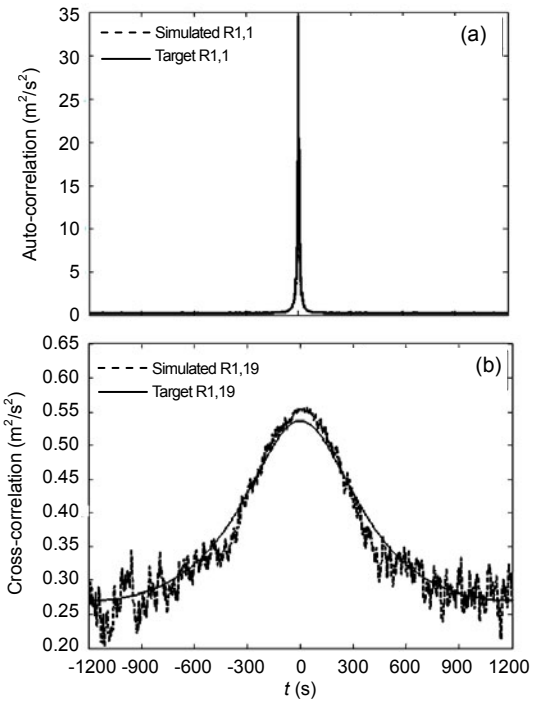

Fig. 13 Comparison of correlation in vertical direction (target: Panofsky spectrum)
(a) Auto-correlation function (point G1); (b) Cross-correlation function (points G1and G19)

$$S_{jm}^{0}(\omega)=\sqrt{S_{jj}^{0}(\omega)S_{mm}^{0}(\omega)}\mathrm{Coh}_{jm}(\Delta_{jm},\omega)\exp[\mathrm{i}\varphi(n^{*})], \tag{33}$$

where the different phase angles $\varphi(n^{*})$ at various locations are empirically expressed as

$$\varphi(n^{*})=\begin{cases}n^{*}\pi/4, & |n^{*}|\le 0.1,\\ -10\pi n^{*}+1.25, & 0.1<|n^{*}|\le 0.125,\\ \text{Random}, & |n^{*}|>0.125,\end{cases} \tag{34}$$

$$n^{*}=2n(Z_i-Z_j)/(U_{Z_i}+U_{Z_j}). \tag{35}$$

From Eqs. (34) and (35), it can be inferred that values of the wind frequency (n) and the height of simulated points (Z_i) are two factors which may lead the spectral density matrix to be non-positive definite. Consider that the simulated points are determined by the finite model, the wind frequency is the dominating factor responsible for the non-positive definite. In this study, the wind frequency is divided into positive domains and non-positive domains with reference to the criteria that would lead Eq. (3) to a positive definite matrix. In positive domains, Eq. (3) could be divided through Cholesky's method directly. In non-positive domains, the divisions could be approximately obtained through interpolation.

5.3.2 Turbulence simulation

Turbulence simulations for towers in along-wind direction are generated based on the modified spectral representation method and the FFT technique. The Davenport coherence function is adopted with λ being 10. The measured spectra and the recommended spectra in current specification (Xiang *et al.*, 2004) are employed to facilitate the comparison. Details involved in the simulation are listed in Table 3.

Table 3 Details for turbulence simulations of girder (each tower)

Parameter	Value	Parameter	Value
Towers' height, H (m)	306	Simulation range, Z (m)	15–315
Number of simulated points, n	10	Upper cutoff frequency, ω_u (rad/s)	10π
Frequency segmentations, N	2048	Sample interval, Δt (s)	0.1
Sample period, T_0 (s)	4096	Simulated time, T_u (s)	1200

The refinement of FFT technology is identical as in the turbulence simulation for the main girder. Turbulence velocities for towers in along-wind direction based on the recommended and fitted spectra are revealed in Fig. 14. Note that the selection of simulated points is points T1 and T5 which are located at the bottom and the middle of the left tower of the Sutong Bridge (Fig. 5).

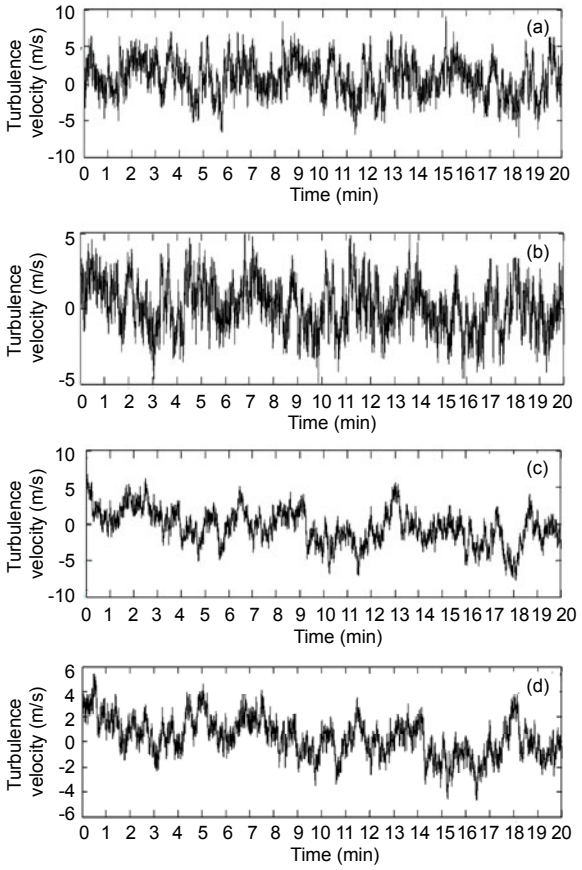

Fig. 14 Simulation of turbulence velocity for towers in along-wind direction

Kaimal (a) and fitted (b) spectra for point T1; Kaimal (c) and fitted (d) spectra for point T5

Comparisons between the simulated spectra of points T1 and T5 (Fig. 5) and the Kaimal spectrum, as well as the simulated spectra of points T1 and T5 and the fitted spectrum in along-wind direction are respectively revealed in Fig. 15 and Fig. 16. It can be concluded that the simulated power spectra of points T1 and T5 match well with Kaimal spectrum or fitted spectrum, signifying the reliability of the measured wind data.

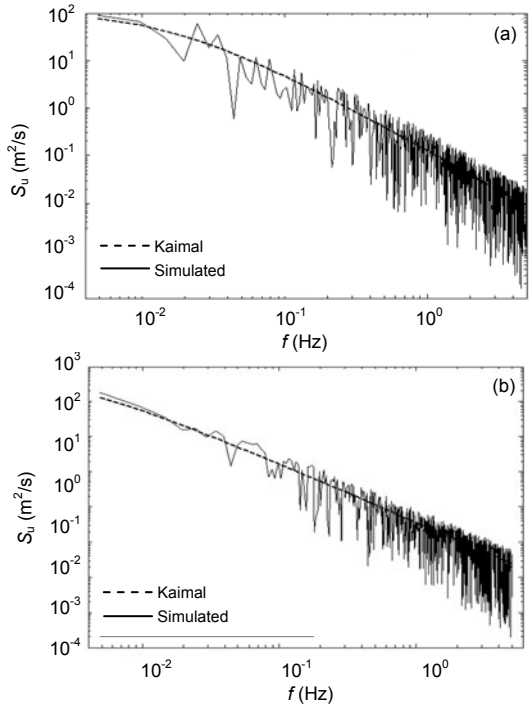

Fig. 15 Comparison of power spectra in along-wind direction
(a) Simulated and Kaimal spectra for point T1; (b) Simulated and Kaimal spectra for point T5

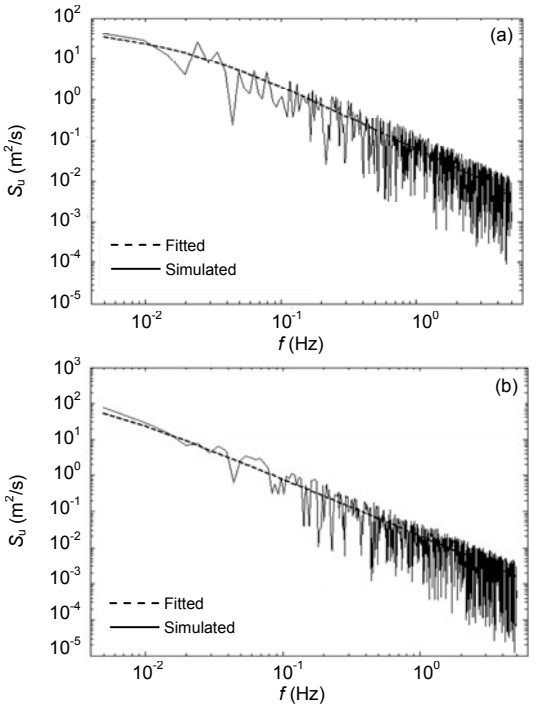

Fig. 16 Comparison of power spectra in along-wind direction
(a) Simulated and fitted spectra for point T1; (b) Simulated and fitted spectra for point T5

Furthermore, comparisons for temporal auto-/cross-correlation functions between generated sample functions and fitting spectra in along-wind direction are shown in Fig. 17. Comparisons of auto-correlation (point T1) and cross-correlation (points T1 and T5) functions indicate apparent deviations between the simulated and target ones. The inaccuracy of the measured wind data and theory formulations adopted for generating sample functions is responsible for the deviations.

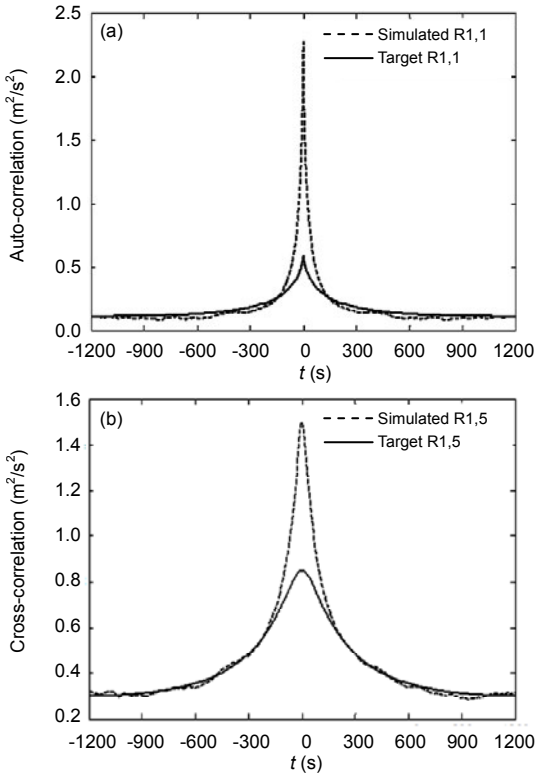

Fig. 17 Comparison of correlation of along-wind direction (target: Kaimal spectra)
(a) Auto-correlation function for point T1; (b) Cross-correlation function for points T1 and T5

6 Summary and conclusions

To facilitate further studies in buffeting behavior of the Sutong Bridge in time domain, turbulence winds are simulated based on the measured wind data from the SHMS. Principles of the spectral representation method and the FFT technique dealing with the stationary stochastic vector process are reviewed. The fitted spectra are obtained from wind data of Typhoon Fung-Wong, Typhoon Kalmaegi and strong winter

winds, collected by the SHMS. Relative comparisons are conducted to validate the reliability and accuracy of the measured data.

Simplifications for turbulence simulations considering the special structural characteristics of long-span bridges are briefly introduced. For a cable-stayed bridge, turbulence wind which is a 3D multi-variate (3D-*n*V) stochastic vector process is converted into four independent 1D univariate (1D-1V) stochastic processes. Turbulence simulations in the along-wind and vertical directions for the main girder and the along-wind direction for the tower are then conducted. The hypothesis for the main girder is applied which assumes the elevation of the overall main girder as being homogeneous. The refinement for the tower is applied which considers the spatial distribution of wind velocity. Comparisons in terms of turbulence velocities, power spectra and auto-/cross-correlation functions between the measured spectra and target spectra (including Kaimal, Panofsky and fitting spectra) are undertaken. The characteristics of simulated turbulences and target ones agree well overall, validating the effectiveness and reliability of the presented turbulence simulation method. The obtained turbulence simulations can provide not only reliable turbulence data for further analysis about the buffeting behavior of the Sutong Bridge, but also references for anti-wind design for other engineering structures in adjacent regions.

References

Bartoli, G., Mannini, C.A., 2008. A simplified approach to bridge deck flutter. *Journal of Wind Engineering and Industrial Aerodynamics*, **96**(2):229-256. [doi:10.1016/j.jweia.2007.06.001]

Beljaars, A.C.M., 1987. The influence of sampling and filtering on measured wind gusts. *American Meteorological Society*, **4**(4):613-626.

Bocciolone, M., Cheli, F., Curami, A., Zasso, A., 1992. Wind measurements on the Humber bridge and numerical simulations. *Journal of Wind Engineering and Industrial Aerodynamics*, **42**(1-3):1393-1404. [doi:10.1016/0167-6105(92)90147-3]

Cao, Y.H., Xiang, H.F., Zhou, Y., 2000. Simulation of stochastic wind velocity field on long-span bridges. *Journal of Engineering Mechanics*, **126**(1):1-6. [doi:10.1061/(ASCE)0733-9399(2000)126:1(1)]

Chen, A.R., 2004. Research on Wind Tunnel Aeroelastic Model of Full Bridge. State Key Laboratory for Disaster Reduction in Civil Engineering, Tongji University, China (in Chinese).

Chen, X., Matsumoto, M., Kareem, A., 2000. Time domain flutter and buffeting response analysis of bridges. *Journal of Engineering Mechanics*, **126**(1):7-16. [doi:10.1061/(ASCE)0733-9399(2000)126:1(7)]

Davenport, A.G., 1962. The buffeting of a suspension bridge by storm winds. *Journal of the Structural Division*, **88**(3):233-270.

Di Paola, M., 1998. Digital simulation of wind field velocity. *Journal of Wind Engineering and Industrial Aerodynamics*, **74-76**:91-109. [doi:10.1016/S0167-6105(98)00008-7]

George, D., 1996. Simulation of ergodic multivariate stochastic processes. *Journal of Engineering Mechanics*, **112**(8):778-787. [doi:10.1061/(ASCE)0733-9399(1996)122:8(778)]

Gurley, K., Kareem, A., 1993. Gust loading factors for tension leg platforms. *Applied Ocean Research*, **15**(3):137-154. [doi:10.1016/0141-1187(93)90037-X]

Han, D.J., Zou, X.J., Su, C., 2003. Simulation of stochastic wind field of long-span bridges considering wind effects of the bridge towers. *Journal of Engineering Mechanics*, **20**(6):18-22 (in Chinese).

Hu, R.M., Wang, H., Li, A.Q., 2010. Measurement study on wind characteristics of Typhoon Kalmaegi on the Sutong Bridge. *Wuhan University Journal of Natural Sciences*, **15**(2):153-159. [doi:10.1007/s11859-010-0213-x]

Kaimal, J.C., Wyngaard, J.C., Izumi, I., Cote, O.R., 1972. Spectral characteristics of surface-layer turbulence. *Quarterly Journal of the Royal Meteorological Society*, **98**(417):563-589. [doi:10.1002/qj.49709841707]

Katsuchi, H., Jones, N.P., Scanlan, R.H., 1999. Multimode coupled flutter and buffeting analysis of the Akashr-kaikyo bridge. *Journal of Structural Engineering*, **125**(1):60-70. [doi:10.1061/(ASCE)0733-9445(1999)125:1(60)]

Kovacs, I., Svensson, H.S., Jordet, E., 1992. Analytical aerodynamic investigation of cable-stayed Helgeland bridge. *Journal of Structural Engineering*, **118**(1):147-168. [doi:10.1061/(ASCE)0733-9445(1992)118:1(147)]

Li, Y., Kareem, A., 1993. Simulation of multivariate random process: hybrid DFT and digital filtering approach. *Journal of Engineering Mechanics*, **119**(5):1078-1098. [doi:10.1061/(ASCE)0733-9399(1993)119:5(1078)]

Liu, C., Huang, S.C., Zhu, X.A., Jiang, Z.H., 2006. Analysis and computation on design wind velocity of Sutong Changjiang highway bridge. *Journal of Applied Meteorological Science*, **17**(1):44-51 (in Chinese).

Niemann, H.J., Hoffer, R., 1995. Nonlinear Effects in the Buffeting Program: a State of the Art in Wind Engineering. Ninth International Conference on Wind Engineering, New Delhi.

Øiseth, O., Rönnquist, A., Sigbjörnsson, R., 2010. Simplified prediction of wind-induced response and stability limit of slender long-span suspension bridge, based on modified quasi-steady theory: A case study. *Journal of Wind Engineering and Industrial Aerodynamics*, **98**(12):730-741. [doi:10.1016/j.jweia.2010.06.009]

Panofsky, H.A., McCormick, R.A., 1960. The spectrum of vertical velocity near the surface. *Quarterly Journal of the Royal Meteorological Society*, **86**(370):495-503.

[doi:10.1002/qj.49708637006]

Scanlan, R.H., 1978. The action of flexible bridges under wind II: Buffeting theory. *Journal of Sound and Vibration*, **60**(2):201-211. [doi:10.1016/S0022-460X(78)80029-7]

Shinozuka, M., 1972. Monte Carlo solution of structural dynamics. *Computers & Structures*, **2**(5-6):855-874. [doi:10.1016/0045-7949(72)90043-0]

Shinozuka, M., Jan, C.M., 1972. Digital simulation of random processes and its applications. *Journal of Sound and Vibration*, **25**(1):111-128. [doi:10.1016/0022-460X(72)90600-1]

Simiu, E., Scanlan, R.H., 1978. Wind Effects on Structures. Wiley, New York.

Strutz, T., 2010. Data Fitting and Uncertainty: A Practical Introduction to Weighted Least Squares and Beyond. Vieweg+Teubner Verlag.

Su, C., Fan., X.M., He, T., 2007. Wind-induced vibration analysis of a cable-stayed bridge during erection by a modified time-domain method. *Journal of Sound and Vibration*, **303**(1-2):330-342. [doi:10.1016/j.jsv.2007.01.018]

Xu, Y.L., Sun, D.K., Ko, J.M., Lin, J.H., 2000. Fully coupled buffeting analysis of TsingMa suspension bridge. *Journal of Wind Engineering and Industrial Aerodynamics*, **85**(1):97-117. [doi:10.1016/S0167-6105(99)00133-6]

Yamazaki, F., Shinozuka, M., 1988. Digital generation of nonGaussian stochastic fields. *Journal of Engineering Mechanics*, **114**(7):1183-1197. [doi:10.1061/(ASCE)0733-9399(1988)114:7(1183)]

Yang, J.N., 1972. Simulation of random envelope processes. *Journal of Sound and Vibration*, **21**(1):73-85. [doi:10.1016/0022-460X(72)90207-6]

Yang, J.N., 1973. On the normality and accuracy of simulated random processes. *Journal of Sound and Vibration*, **26**(3):417-428. [doi:10.1016/S0022-460X(73)80196-8]

Yang, W.W., Chang, T.Y.P., Chang, C.C., 1997. An efficient wind field simulation technique for bridges. *Journal of Wind Engineering and Industrial Aerodynamics*, **67-68**:697-708. [doi:10.1016/S0167-6105(97)00111-6z]

Xiang, H.F., Bao, W.G., Chen, A.R., Lin, Z.X., Liu, J.X., 2004. Wind-Resistant Design Specification for Highway Bridges. China Communications Press, Beijing (in Chinese).

Wang, H., Li, A.Q., Jiao, C.K., 2010a. Characteristics of strong winds at the Runyang Suspension Bridge based on field tests from 2005 to 2008. *Journal of Zhejiang University-SCIENCE A (Applied Physics and Engineering)*, **11**(7):465-476. [doi:10.1631/jzus. A0900601]

Wang, H., Li, A.Q., Zhao, G.W., Li, J., 2010b. Non-linear buffeting response analysis of long-span suspension bridges with central buckle. *Earthquake Engineering and Engineering Vibration*, **9**(2):259-270. [doi:10.1007/s11803-010-0011-7]

Wang, H., Li, A.Q., Hu, R.M., 2011. Comparison of ambient vibration response of the Runyang Suspension Bridge under skew winds with time-domain numerical predictions. *Journal of Bridge Engineering*, **16**(4):513-526. [doi:10.1061/(ASCE)BE.1943-5592.0000168]

2010 JCR of Thomson Reuters for *JZUS-A* and *JZUS-B*

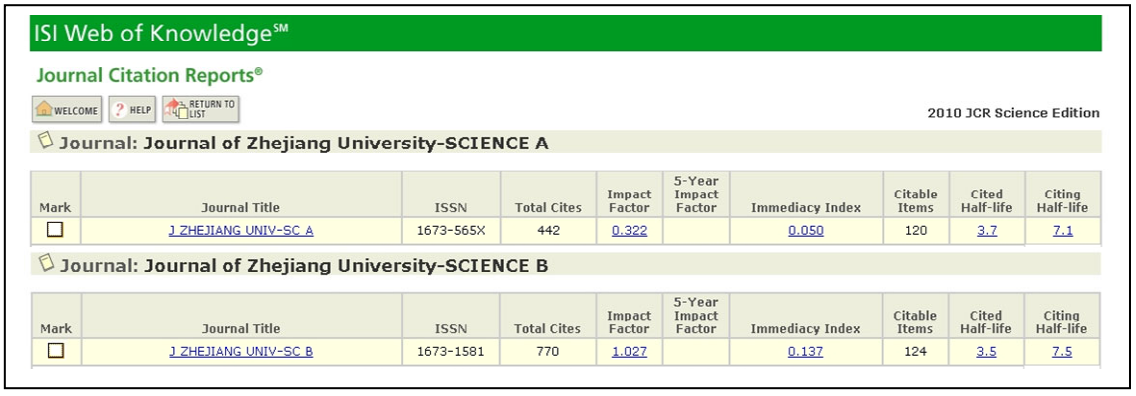

ISI Web of Knowledge℠

Journal Citation Reports®

WELCOME | HELP | RETURN TO LIST

2010 JCR Science Edition

Journal: Journal of Zhejiang University-SCIENCE A

Mark	Journal Title	ISSN	Total Cites	Impact Factor	5-Year Impact Factor	Immediacy Index	Citable Items	Cited Half-life	Citing Half-life
☐	J ZHEJIANG UNIV-SC A	1673-565X	442	0.322		0.050	120	3.7	7.1

Journal: Journal of Zhejiang University-SCIENCE B

Mark	Journal Title	ISSN	Total Cites	Impact Factor	5-Year Impact Factor	Immediacy Index	Citable Items	Cited Half-life	Citing Half-life
☐	J ZHEJIANG UNIV-SC B	1673-1581	770	1.027		0.137	124	3.5	7.5